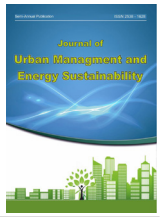
*Int. J. Urban Manage. Energy Sustainability, 7(3):337-349, 2026*

International Journal of Urban Management and Energy Sustainability (IJUMES)

Homepage: http://www.ijumes.com



CASE STUDY RESEARCH PAPER

# Assessment of Sustainable High-performance Cementitious Concrete Incorporating Nano silica and Aluminum Sulphate for Multiscale Urban Engineering Application

Amirhossein Hojati, Aliasghar Amirkardoust*, Davood Sedaghat Shayegan, Razieh Sistaninejad

*Department of Civil Engineering, RO.C., Islamic Azad University, Roudehen, Iran*

ARTICLE INFO

*Article History:*
Received 2026-05-01
Revised 2026-07-10
Accepted 2026-08-25

*Keywords:*
Aluminum sulfate; AR glass fiber; mechanical properties; Nano-silica; Slag–cement concrete; urban infrastructure

ABSTRACT

Improving the mechanical performance of slag–cement concrete is important for durable and resource-efficient urban infrastructure. This study investigates the combined effects of nano-silica, aluminum sulfate, and alkali-resistant glass fibers on the mechanical properties of concrete containing Portland cement and ground granulated blast furnace slag. Nineteen mixtures were prepared with a constant binder content of 530 kg/m³ and a water-to-binder ratio of 0.33. NS replaced GGBS at 10, 20, and 30 kg/m³, AS was added at nominal dosages of 4% and 8%, and AR glass fibers were incorporated at volume fractions of 0.4%, 0.6%, and 0.8%. Compressive strength was measured at 14 and 28 days, and splitting tensile and flexural strengths were measured at 28 days. All modified mixtures outperformed the control mixture. The mixture containing 30 kg/m³ NS, 8% AS, and 0.8% fibers achieved the highest 28-day compressive strength, approximately 41% higher than that of the control mixture, as well as the highest splitting tensile and flexural strengths, corresponding to increases of approximately 74% and 77%, respectively. NS content governed compressive strength, whereas fiber content governed tensile and flexural strengths. The results indicate that combining NS, AS, and AR glass fibers in slag–cement concrete is a promising strategy for producing high-strength concrete for structural elements in urban infrastructure, subject to confirmation of its durability and microstructural performance.

DOI: 10.22034/ijumes.2026.743388

*Running Title: Sustainable High-performance Cementitious Concrete*

| NUMBER OF REFERENCES | NUMBER OF FIGURES | NUMBER OF TABLES |
|---|---|---|
| 28 | 09 | 03 |

*Corresponding Author:
Email: *al.amirkardoust@iau.ac.ir*
*Phone: 00982176507660*
ORCID: https://orcid.org/0000-0002-1960-9671

## INTRODUCTION

The increasing demand for resilient, sustainable, and high-performance infrastructure in growing cities has accelerated the development of advanced cementitious composites that can satisfy structural, durability, and service-life requirements under increasingly aggressive environmental conditions (Wang et al., 2021). Conventional high-performance concrete (HPC), despite its high compressive strength and low permeability, exhibits several intrinsic deficiencies associated with its dense cementitious matrix (Tahwia et al., 2022), including high autogenous shrinkage, pronounced brittleness, and susceptibility to early-age cracking (Hiew et al., 2026). These limitations restrict the long-term reliability of HPC in critical infrastructure such as high-rise buildings, long-span bridges, marine structures, and transportation systems, where mechanical performance alone is insufficient to ensure structural integrity throughout the design life (Wang et al., 2024). Fiber reinforcement is one of the most effective strategies for overcoming the brittle behavior of HPC. Among the available fibers, alkali-resistant (AR) glass fibers combine a relatively high elastic modulus with immunity to electrochemical corrosion, and their zirconia content protects them against degradation in the alkaline pore solution of cementitious matrices (Bentur & Mindess, 2007). Their main strengthening mechanisms are crack bridging, stress redistribution, and suppression of crack propagation from the micro- to the macro-scale, which improve the tensile strength, flexural strength, and toughness of cementitious composites (Hiew et al., 2026). Nevertheless, fiber incorporation introduces several challenges. Weak interfacial bonding between the fibers and the hydrated cement paste limits stress transfer, and fiber agglomeration, reduced workability, and entrapped air compromise the homogeneity of the composite (Hussein et al., 2022). Consequently, fibers alone cannot optimize the matrix microstructure required for high-strength concrete. In recent years, nanotechnology has emerged as an effective approach for tailoring the microstructure of cement-based materials (Ghafari et al., 2015). Among the various nanomaterials, nano-silica is particularly effective because of its dual physical and chemical functions in hydrating cement systems. Physically, nano-silica particles act as ultrafine fillers that occupy nanoscale voids between cement grains, refining the pore structure and increasing matrix compactness. Chemically, their high specific surface area and amorphous silica content promote rapid pozzolanic reactions with the calcium hydroxide released during cement hydration, generating additional calcium silicate hydrate (C–S–H), the principal binding phase responsible for strength (Khan et al., 2022). Nano-silica particles also act as nucleation sites that accelerate early hydration, leading to a denser and more homogeneous distribution of hydration products. Accordingly, silica-based additions have been reported to improve the compressive, tensile, and flexural strengths of concrete (Nazari et al., 2026; Raveendran & Krishnan, 2025). However, the high specific surface area of nano-silica increases water demand and may increase autogenous shrinkage, and poor dispersion can lead to agglomeration and localized defects (Vargas et al., 2024). Shrinkage remains a critical factor in high-strength concrete: as the water-to-binder ratio decreases and the binder content increases, self-desiccation produces significant autogenous shrinkage at early ages, while drying shrinkage contributes to tensile stresses and microcracking over time (Li & Yao, 2001; Afroughsabet & Teng, 2020). Sulfate- and sulfoaluminate-based modifiers have therefore attracted interest as shrinkage-compensating admixtures. Their primary mechanism is the rapid formation of expansive ettringite during early hydration, which compensates for autogenous and drying shrinkage while refining the microstructure (Sirtoli et al., 2019, 2020). When properly proportioned, such admixtures can also accelerate strength development and improve the mechanical properties of fiber-reinforced composites (Choi & Yun, 2013; Qadri et al., 2024), whereas excessive dosages

may cause internal stresses and microcracking (Mehdipour & Khayat, 2018).

Recent investigations have explored binary combinations of fibers and nanoparticles, or of nanoparticles and expansive agents, to exploit synergistic interactions between different reinforcing mechanisms (Hussein et al., 2022; Piao et al., 2023). In principle, integrating these mechanisms in a single cementitious system could establish a hierarchical reinforcement strategy operating across multiple length scales (Wang et al., 2024): at the nanoscale, additional C–S–H generated by nano-silica increases matrix density; at the microscale, ettringite formation compensates for shrinkage and improves interfacial integrity; and at the macroscale, fibers arrest crack propagation and increase energy absorption. Despite this potential, important gaps remain. Most existing studies have investigated fibers, nano-silica, or sulfate-based modifiers individually, and investigations of their combined effects in high-strength concrete are limited (Ren et al., 2024; Xuan & Wang, 2022). In particular, the combined influence of nano-silica replacement of GGBS, aluminum sulfate dosage, and AR glass fiber content on the compressive, splitting tensile, and flexural strengths of slag–cement concrete has not been systematically quantified (Wang & Sadeghzadeh, 2025). The present study addresses this gap through a systematic experimental program on slag–cement concrete modified with nano-silica, aluminum sulfate, and AR glass fibers. Nineteen mixtures were designed by varying the nano-silica content (10, 20, and 30 kg/m³ replacing GGBS), the aluminum sulfate dosage (4% and 8%), and the fiber volume fraction (0.4%, 0.6%, and 0.8%), and their compressive strength (14 and 28 days) and splitting tensile and flexural strengths (28 days) were evaluated. The working hypothesis is that nano-silica primarily densifies the matrix and governs compressive strength, aluminum sulfate refines the early hydration structure, and AR glass fibers primarily govern tensile and flexural performance, so that their combination improves all three mechanical properties. The study focuses on mechanical performance; shrinkage, durability, and microstructural characterization are identified as subjects for future work.

## MATERIALS AND METHODS

*Binder materials:* Type II ordinary Portland cement (OPC) conforming to ASTM C150/C150M-11 (ASTM International, 2011), with a specific gravity of 3.15, was used as the primary binder. Ground granulated blast furnace slag (GGBS), an industrial by-product, was used as a supplementary cementitious material (SCM). Owing to its latent hydraulic nature, GGBS reacts gradually in the highly alkaline pore solution generated during cement hydration to produce secondary C–S–H, thereby reducing porosity, improving long-term strength, and enhancing resistance to chloride penetration and sulfate attack (Raghav et al., 2021). The GGBS, with a specific gravity of 2.66, was sourced from Foolad Mobarakeh, Isfahan, Iran. Nano-silica (NS) was used to partially replace GGBS. Unlike GGBS, NS exhibits very high pozzolanic activity owing to its amorphous structure, nanoscale particle size, and large specific surface area; it accelerates cement hydration by providing nucleation sites for C–S–H precipitation while consuming calcium hydroxide to form additional binding phases (Khan et al., 2022). Limestone powder (LSP) was used as a micro-filler to improve particle packing. The chemical compositions of the cement, LSP, GGBS, and NS are given in (Tab. 1), and the binder constituents are shown in (Fig. 1).

*Aggregates:* The coarse aggregate was angular crushed gravel with a nominal maximum size of 12.5 mm, and the fine aggregate was silica sand. Their grading curves are shown in (Fig. 2), and their physical properties are listed in (Tab. 2). The apparent specific gravities of the coarse and fine aggregates were 2.72 and 2.71, and their water absorptions were 0.44% and 1.36%, respectively.

Table 1: Chemical composition (wt.%) and specific gravity of the binder materials and limestone powder

| Oxide | Cement | LSP | GGBS | NS |
|---|---|---|---|---|
| $SiO_2$ | 20.68 | 0.45 | 32.57 | ≥ 99 |
| $Al_2O_3$ | 4.51 | 4.86 | 1.26 | - |
| $Fe_2O_3$ | 4.13 | 3.30 | 3.3 | - |
| CaO | 63.66 | 63.33 | 34.07 | - |
| MgO | 1.35 | 1.15 | 0.89 | - |
| $SO_3$ | 2.55 | 2.10 | 0.5 | - |
| $Na_2O$ | 0.26 | - | 1.12 | - |
| $K_2O$ | 0.74 | - | 0.56 | - |
| LOI | 2.50 | - | 2.28 | 0.2 |
| Specific gravity | 3.15 | – | 2.66 | – |

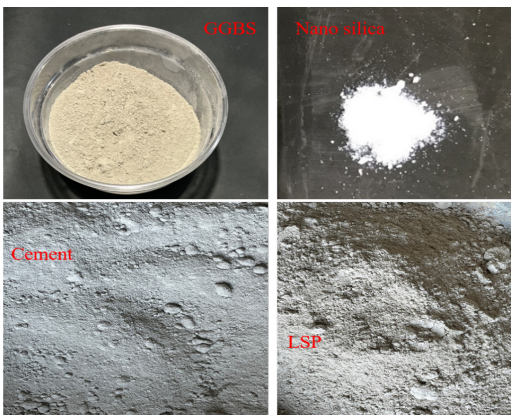



Figure 1: Binder constituents: (a) OPC, (b) GGBS, (c) nano-silica, and (d) limestone powder.

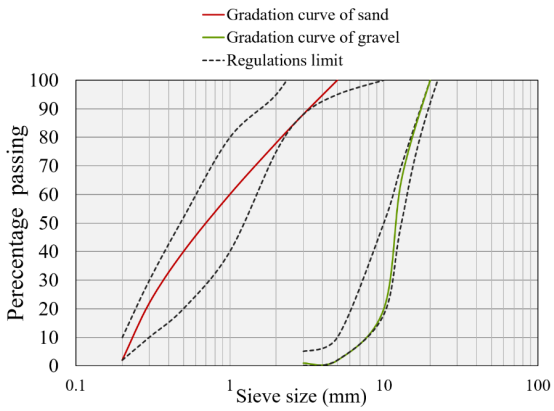



Figure 2: Grading curves of the aggregates.

Table 2: Physical properties of the aggregates

| Properties | Gravel | Silica sand |
|---|---|---|
| Apparent specific gravity | 2.72 | 2.71 |
| Density (OD) (kg/m3) | 2680 | 2609 |
| Density (SSD) (kg/m3) | 2691 | 2644 |
| Bulk density (kg/m3) | 1466 | 1493 |
| Water absorption (%) | 0.44 | 1.36 |
| Los Angeles abrasion value (%) | 13.98 | - |

*Superplasticizer:* A polycarboxylate-ether (PCE) superplasticizer with a density of 1.05 g/cm³ at 20 °C, a pH of 5.0, and a dry residue of 37.0% was used to improve fluidity and workability. A constant dosage of 8.5 kg/m³, corresponding to 1.6% of the binder mass, was used in all mixtures.

Alkali-resistant (AR) glass fibers: AR glass fibers manufactured by UNINK New Materials Co., Ltd. (China) were used as discrete reinforcement to improve the tensile behavior and crack

resistance of the concrete. Unlike conventional E-glass fibers, AR glass fibers contain zirconium dioxide, which enhances their chemical stability by limiting degradation caused by hydroxyl ions in the cement pore solution (Bentur & Mindess, 2007).

The fibers had a nominal length of 6 mm, a diameter of 18 µm, a density of 2.56 g/cm³, a tensile strength of 442 MPa, and negligible water absorption.

Aluminum sulfate: Aluminum sulfate powder ($Al_2(SO_4)_3$), supplied by Strumix Co. (Iran) as a fine white powder of high purity, was used as a sulfate-bearing chemical modifier to promote early hydration reactions (Fig. 3).

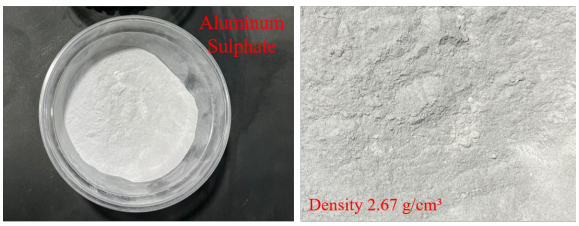



Figure 3: Aluminum sulfate powder.

Aluminum sulfate is highly water-soluble and readily dissociates in the mixing water, releasing $Al^{3+}$ and $SO_4^{2-}$ ions. In Portland cement systems, these ions react with tricalcium aluminate ($C_3A$) and calcium hydroxide to promote the formation of ettringite (AFt) during early hydration. Controlled ettringite crystallization can produce moderate internal expansion that compensates for autogenous shrinkage and reduces early-age microcracking, while the accelerated formation of hydration products refines the pore structure (Choi & Yun, 2013; Mehdipour & Khayat, 2018). The effectiveness of sulfate-bearing modifiers depends strongly on their dosage: moderate additions promote controlled expansion and hydration acceleration, whereas excessive amounts may cause excessive ettringite formation, internal stresses, and microstructural instability (Choi & Yun, 2013). The dosages adopted in this study were therefore limited to two moderate levels.

*Mix Design, Specimen Preparation, and Testing*

The mixtures were designed to investigate the combined influence of NS, aluminum sulfate (AS), and AR glass fibers on the mechanical properties of high-strength concrete. A total of 19 mixtures were prepared, comprising one control mixture and 18 modified mixtures in a full factorial design (3 NS contents × 2 AS dosages × 3 fiber contents); the mixture proportions are presented in Table 3. The total binder content was kept constant at 530 kg/m³ and the water-to-binder ratio (w/b) at 0.33. The cement content was kept constant at 330 kg/m³, whereas the GGBS content was reduced from 200 to 190, 180, and 170 kg/m³ by replacing it with 10, 20, and 30 kg/m³ of NS (1.9%, 3.8%, and 5.7% of the binder mass), respectively. AS was added at nominal dosages of 4% and 8%, corresponding to 20.6 and 41.2 kg/m³ (approximately 3.9% and 7.8% of the binder mass). AR glass fibers were added at volume fractions of 0.4%, 0.6%, and 0.8%, corresponding to 10.2, 15.4, and 20.5 kg/m³. The contents of silica sand (750 kg/m³), crushed gravel (850 kg/m³), limestone powder (60 kg/m³), and PCE superplasticizer (8.5 kg/m³) were kept constant. Each mixture is designated by its NS content (kg/m³), AS dosage (%), and fiber volume fraction (%); for example, 30NS-8AS-0.8F denotes the mixture containing 30 kg/m³ NS, 8% AS, and 0.8% fibers.

*Mixing Procedure*

All mixtures were prepared in a 60-L laboratory pan mixer. Before mixing, all dry materials were conditioned to the laboratory temperature (23 ± 2 °C). The cement, GGBS, NS, limestone powder, and aluminum sulfate were first dry-mixed for approximately 2 min to ensure a homogeneous distribution of the binder constituents. The silica sand and coarse aggregate were then added and mixed for a further 2 min. Approximately 80% of the mixing water, containing the pre-dissolved superplasticizer, was gradually introduced while mixing continued for 3 min, after which the remaining water was added. Finally, the AR glass fibers were gradually dispersed into the fresh concrete over approximately 2 min to minimize

Table 3: Mixture proportions (kg/m³ unless otherwise stated)

| Mix No. | Mix ID | Cement | GGBS | NS | Total binder | AS (%) | AS | Water | w/b | PCE SP | Silica sand | Gravel | LSP | AR glass fiber (vol.%) |
|---|---|---|---|---|---|---|---|---|---|---|---|---|---|---|
| 1 | Control | 330 | 200 | 0 | 530 | 0 | 0.00 | 175 | 0.33 | 8.5 | 750 | 850 | 60 | 0 |
| 2 | 10NS-4AS-0.4F | 330 | 190 | 10 | 530 | 4% | 20.60 | 175 | 0.33 | 8.5 | 750 | 850 | 60 | 0.4 |
| 3 | 10NS-4AS-0.6F | 330 | 190 | 10 | 530 | 4% | 20.60 | 175 | 0.33 | 8.5 | 750 | 850 | 60 | 0.6 |
| 4 | 10NS-4AS-0.8F | 330 | 190 | 10 | 530 | 4% | 20.60 | 175 | 0.33 | 8.5 | 750 | 850 | 60 | 0.8 |
| 5 | 20NS-4AS-0.4F | 330 | 180 | 20 | 530 | 4% | 20.60 | 175 | 0.33 | 8.5 | 750 | 850 | 60 | 0.4 |
| 6 | 20NS-4AS-0.6F | 330 | 180 | 20 | 530 | 4% | 20.60 | 175 | 0.33 | 8.5 | 750 | 850 | 60 | 0.6 |
| 7 | 20NS-4AS-0.8F | 330 | 180 | 20 | 530 | 4% | 20.60 | 175 | 0.33 | 8.5 | 750 | 850 | 60 | 0.8 |
| 8 | 30NS-4AS-0.4F | 330 | 170 | 30 | 530 | 4% | 20.60 | 175 | 0.33 | 8.5 | 750 | 850 | 60 | 0.4 |
| 9 | 30NS-4AS-0.6F | 330 | 170 | 30 | 530 | 4% | 20.60 | 175 | 0.33 | 8.5 | 750 | 850 | 60 | 0.6 |
| 10 | 30NS-4AS-0.8F | 330 | 170 | 30 | 530 | 4% | 20.60 | 175 | 0.33 | 8.5 | 750 | 850 | 60 | 0.8 |
| 11 | 10NS-8AS-0.4F | 330 | 190 | 10 | 530 | 8% | 41.20 | 175 | 0.33 | 8.5 | 750 | 850 | 60 | 0.4 |
| 12 | 10NS-8AS-0.6F | 330 | 190 | 10 | 530 | 8% | 41.20 | 175 | 0.33 | 8.5 | 750 | 850 | 60 | 0.6 |
| 13 | 10NS-8AS-0.8F | 330 | 190 | 10 | 530 | 8% | 41.20 | 175 | 0.33 | 8.5 | 750 | 850 | 60 | 0.8 |
| 14 | 20NS-8AS-0.4F | 330 | 180 | 20 | 530 | 8% | 41.20 | 175 | 0.33 | 8.5 | 750 | 850 | 60 | 0.4 |
| 15 | 20NS-8AS-0.6F | 330 | 180 | 20 | 530 | 8% | 41.20 | 175 | 0.33 | 8.5 | 750 | 850 | 60 | 0.6 |
| 16 | 20NS-8AS-0.8F | 330 | 180 | 20 | 530 | 8% | 41.20 | 175 | 0.33 | 8.5 | 750 | 850 | 60 | 0.8 |
| 17 | 30NS-8AS-0.4F | 330 | 170 | 30 | 530 | 8% | 41.20 | 175 | 0.33 | 8.5 | 750 | 850 | 60 | 0.4 |
| 18 | 30NS-8AS-0.6F | 330 | 170 | 30 | 530 | 8% | 41.20 | 175 | 0.33 | 8.5 | 750 | 850 | 60 | 0.6 |
| 19 | 30NS-8AS-0.8F | 330 | 170 | 30 | 530 | 8% | 41.20 | 175 | 0.33 | 8.5 | 750 | 850 | 60 | 0.8 |

agglomeration, and mixing was continued for a further 3 min, giving a total mixing time of approximately 12–14 min per batch. The fresh concrete was visually inspected to confirm uniform fiber dispersion without fiber balling or segregation. The specimens (Fig. 4) comprised (a) 100 mm cubes for compressive strength, (b) 100 × 100 × 500 mm prisms for flexural strength, and (c) 150 × 300 mm cylinders for splitting tensile strength (British Standards Institution, 2021).

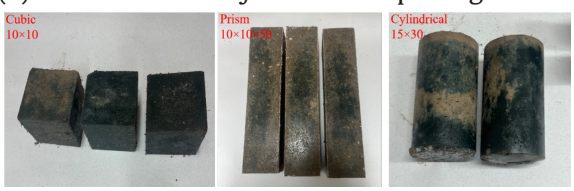



Figure 4: Concrete specimens: (a) cubes, (b) prisms, and (c) cylinders.

*Casting and Curing*

Immediately after mixing, the fresh concrete was placed in lubricated steel molds in two equal layers, each compacted on a vibrating table for approximately 15–20 s to remove entrapped air without causing segregation. The top surface was finished with a steel trowel and covered with a plastic sheet to prevent moisture loss. After 24 ± 2 h, the specimens were demolded and cured in lime-saturated water at 23 ± 2 °C until testing (Fig. 5) (ASTM International, 2012). Compressive strength was determined at 14 and 28 days, and splitting tensile and flexural strengths were determined at 28 days.




Figure 5: Prepared specimens and water curing.

*Test Methods*

Compressive strength was determined on cube specimens in accordance with BS EN 12390-3 (British Standards Institution, 2019), splitting tensile strength on cylinders in accordance with ASTM C496/C496M (ASTM International, 2017), and flexural strength on prisms under three-point loading in accordance with ASTM C293/C293M (ASTM International, 2016).

## FINDINGS AND DISCUSSION

*Compressive Strength*

The compressive strength results are presented in (Fig. 6). The control mixture exhibited compressive strengths of 39.61 and 45.24 MPa at 14 and 28 days, respectively. Replacing part of the GGBS with NS increased compressive strength regardless of the AS dosage or fiber content. At 4% AS and 0.4% fibers, increasing the NS content from 10 to 30 kg/m³ increased the 28-day compressive strength from 53.07 to 60.03 MPa (approximately 13.1%), corresponding to an improvement of approximately 32.7% over the control. A similar trend was observed for mixtures containing 0.6% fibers, for which the strength increased from 53.94 to 60.90 MPa (approximately 12.9%), and for mixtures containing 0.8% fibers, for which it increased from 54.81 to 61.77 MPa (approximately 12.7%). These results indicate that NS consistently enhanced compressive strength irrespective of fiber content, suggesting that its contribution originated mainly from modification of the cementitious matrix. The strength development between 14 and 28 days at each NS level is shown in (Fig. 7).

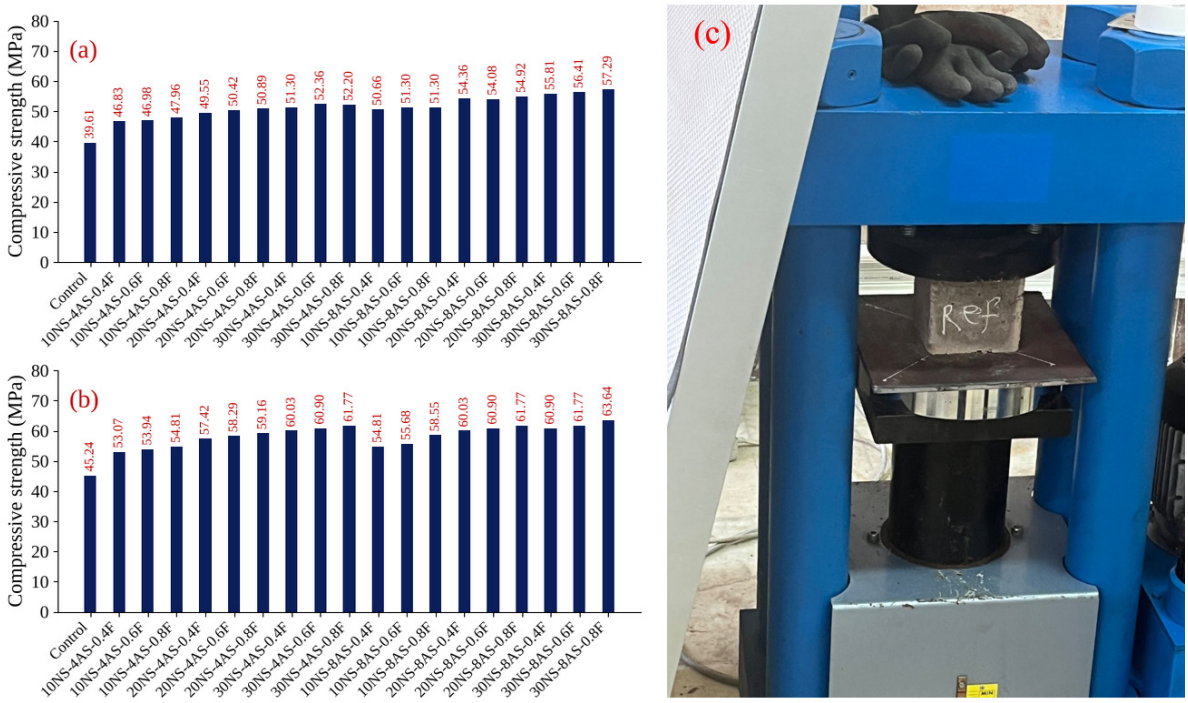



Figure 6: Compressive strength results: (a) 14 days, (b) 28 days, and (c) test setup.

The observed enhancement can be explained by three complementary mechanisms. First, the nanosized particles occupy voids between cement grains and hydration products, producing a filler effect that reduces capillary porosity. Because NS particles are considerably smaller than cement particles, they fill interstitial spaces that are inaccessible to larger particles, improving packing density and reducing pore connectivity. Second, NS acts as heterogeneous nucleation sites for C–S–H; owing to its very high specific surface area, it accelerates cement hydration during the first hours after mixing and promotes a more homogeneous microstructure (Khan et al., 2022).

Third, NS participates in the pozzolanic reaction:

$$SiO_2 + Ca(OH)_2 + H_2O \rightarrow C\text{-}S\text{-}H \quad (1)$$

in which calcium hydroxide generated during cement hydration is consumed to produce additional C–S–H gel. The secondary C–S–H generally has a lower Ca/Si ratio and a denser structure than the primary hydration products, increasing stiffness and compressive strength. These mechanisms are expected to reduce the thickness and porosity of the interfacial transition zone (ITZ) around aggregates and fibers; because the ITZ is traditionally the weakest region in concrete, its improvement enhances load transfer under compression (Ghafari et al., 2015; Khan et al., 2022). In the present study, the highest NS dosage corresponded to 5.7% of the binder mass, which exceeds the optimum of approximately 2–3% frequently reported for nano-silica (Khan et al., 2022). Nevertheless, no reduction in strength was observed within the investigated range, possibly because the NS replaced GGBS rather than cement and because the PCE superplasticizer aided dispersion; microstructural analysis is required to confirm this interpretation.

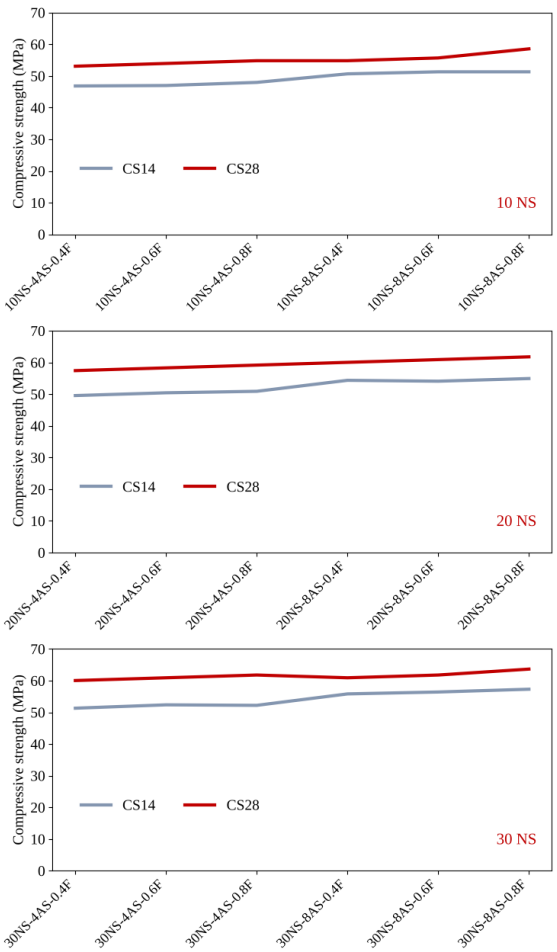



Figure 7: Compressive strength at 14 and 28 days of the mixtures containing 10, 20, and 30 kg/m³ nano-silica.

*Effect of Aluminum Sulfate*

Increasing the AS dosage from 4% to 8% further enhanced strength development. For mixtures containing 10 kg/m³ NS and 0.4% fibers, the 28-day compressive strength increased from 53.07 to 54.81 MPa (approximately 3.3%). At 20 kg/m³ NS, the corresponding increase was from 57.42 to 60.03 MPa (approximately 4.5%). At 30 kg/m³ NS, the strength increased from 60.03 to 60.90 MPa for 0.4% fibers and reached 63.64 MPa when combined with 0.8% fibers, the highest value in the experimental program. The beneficial influence of AS is attributed mainly to accelerated

ettringite formation during early hydration: dissolved sulfate and aluminum ions react with $C_3A$ to form finely distributed ettringite crystals that occupy pore space and contribute to early matrix densification. Controlled ettringite formation may also partially compensate for autogenous shrinkage, reducing early-age microcracks that would otherwise impair later strength, and early ettringite crystals may provide additional nucleation sites for subsequent hydration.

Unlike excessive expansive agent dosages, which may generate detrimental internal stresses, the AS dosages adopted in this study did not reduce strength at any NS or fiber level, suggesting that any expansion remained within non-detrimental limits. This is consistent with Choi and Yun (2013), who reported that calcium sulfoaluminate-based expansive admixtures improved the mechanical properties of fiber-reinforced cement composites up to an optimum replacement level, beyond which excessive expansion reduced compressive strength. Expansion and shrinkage measurements are required to confirm this mechanism directly.

*Effect of AR Glass Fibers*

The incorporation of AR glass fibers produced additional, although smaller, improvements in compressive strength. For mixtures containing 30 kg/m³ NS and 8% AS, increasing the fiber content from 0.4% to 0.8% increased the compressive strength from 60.90 to 63.64 MPa (approximately 4.5%), and at 4% AS it increased from 60.03 to 61.77 MPa (approximately 2.9%). The modest contribution of fibers is expected, because compressive failure is governed primarily by matrix crushing rather than tensile crack opening. Nevertheless, fibers delay the coalescence of microcracks that develop under compressive loading: by bridging inclined cracks and redistributing localized stresses, they postpone unstable crack propagation and increase the energy required for failure. In addition, the relatively high elastic modulus of glass fibers allows them to provide more effective confinement than low-modulus polymer fibers, while their alkali-resistant composition ensures stability in the alkaline cement matrix (Bentur & Mindess, 2007).

At 4% AS, the fiber-induced increase in compressive strength was the same at all NS levels (approximately 1.7 MPa from 0.4% to 0.8% fibers), indicating that, under compression, the contributions of NS and fibers were largely additive. Under tensile and flexural loading, however, a denser matrix and ITZ are expected to improve the fiber–matrix bond and stress transfer (Bentur & Mindess, 2007), as discussed in the following sections.

*Combined Effect of Nano-Silica, Aluminum Sulfate, and AR Glass Fibers*

The compressive strength results indicate that the three modifiers contributed through different mechanisms:

•Nano-silica refines the pore structure and contributes to pozzolanic C–S–H formation;

•Aluminum sulfate promotes early ettringite formation and early matrix densification;

•AR glass fibers bridge microcracks and delay unstable crack propagation.

When incorporated together, these mechanisms operate at different length scales: at the nanometer scale, NS increases the density of hydration products; at the micrometer scale, AS modifies the early hydration chemistry; and at the millimeter scale, fibers arrest crack propagation and redistribute stresses. The highest compressive strength (63.64 MPa, approximately 40.7% above the control) was obtained when the highest dosages of all three modifiers were combined, and the continuous increase in strength without any decline indicates that the selected dosage ranges remained below the levels at which NS agglomeration or excessive ettringite expansion becomes detrimental.

Because the experimental program did not include mixtures containing only one of the three modifiers, the individual contribution of each modifier relative to the control cannot be isolated, and the term “combined effect” is therefore

used rather than “synergy”. Within the factorial design, NS content had the largest influence on compressive strength (approximately 5.1–7.0 MPa between 10 and 30 kg/m³), followed by fiber content (approximately 1.7–3.7 MPa between 0.4% and 0.8%) and AS dosage (approximately 0.9–3.7 MPa between 4% and 8%).

*Splitting Tensile Strength*

The splitting tensile strength results (Fig. 8) followed trends similar to those of compressive strength. The control mixture achieved a splitting tensile strength of 3.8 MPa, whereas the modified mixtures exhibited values of 4.8–6.6 MPa, corresponding to improvements of 26–74%.

Increasing the NS content from 10 to 30 kg/m³ increased the tensile strength at all AS and fiber levels. At 4% AS and 0.8% fibers, the tensile strength increased from 5.6 to 6.2 MPa, and the corresponding mixtures containing 8% AS reached 5.7–6.6 MPa. This improvement is attributed mainly to matrix refinement and reduced pore connectivity resulting from the filler effect and pozzolanic reaction of NS, which also strengthen the ITZ and improve stress transfer between the aggregates, fibers, and paste. Unlike compressive strength, tensile strength was highly sensitive to fiber content: increasing the fiber content from 0.4% to 0.8% increased the tensile strength by approximately 16–21%, indicating that crack bridging became a dominant mechanism under tensile loading. During splitting, tensile stresses induce rapid crack initiation, and the embedded fibers bridge the developing cracks, redistribute stresses, and delay unstable crack propagation. The fiber-induced increase was slightly larger at higher NS contents (0.8 MPa at 10 kg/m³ NS versus 0.9–1.1 MPa at 20–30 kg/m³ NS), consistent with an improved fiber–matrix bond in a denser matrix (Bentur & Mindess, 2007). The effect of increasing the AS dosage from 4% to 8% was small (0.1–0.4 MPa). The highest tensile strength (6.6 MPa) was achieved by the 30NS-8AS-0.8F mixture.

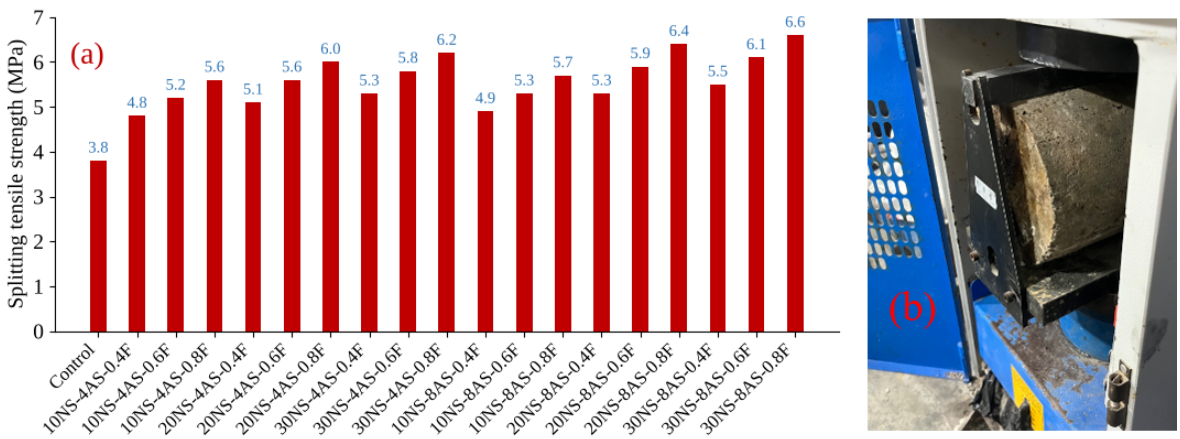



Figure 8: Splitting tensile strength: (a) 28-day results and (b) test setup.

These findings agree with previous studies reporting that nano-silica and fibers have complementary effects on tensile behavior through the simultaneous enhancement of matrix density and crack resistance (Hussein et al., 2022; Raveendran & Krishnan, 2025).

*Flexural Strength*

Flexural strength is particularly sensitive to crack initiation and propagation and therefore provides a direct assessment of the effectiveness of fiber reinforcement. As shown in (Fig. 9), the flexural strength increased from 6.2 MPa for the control mixture to a maximum of 11.0 MPa for the 30NS-8AS-0.8F mixture, an increase of approximately 77%. Increasing the NS content consistently enhanced flexural strength because of the denser matrix and stronger fiber–matrix

bond, which enable more efficient stress transfer from the matrix to the fibers and delay fiber pull-out during bending.

Among the investigated parameters, fiber content had the greatest influence on flexural performance: increasing the fiber content from 0.4% to 0.8% increased the flexural strength by approximately 16–21%, confirming that fiber bridging effectively controlled crack opening under bending. This behavior is consistent with the failure mechanism of fiber-reinforced concrete, in which fibers continue to transfer tensile stresses across cracked sections after matrix cracking (Bentur & Mindess, 2007).

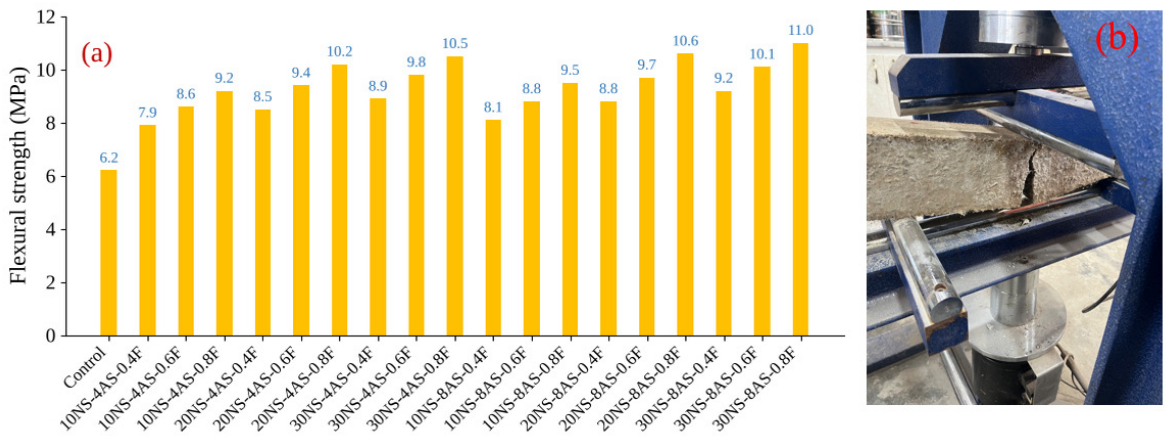



Figure 9: Flexural strength: (a) 28-day results and (b) three-point bending test setup.

Consequently, the combined action of NS, AS, and AR glass fibers produced a crack-resistant composite capable of sustaining higher tensile stresses before failure, consistent with reported improvements in the flexural behavior of nano-modified fiber-reinforced cementitious composites (Hussein et al., 2022).

*Effect of Aluminum Sulfate on Flexural Strength*

Increasing the AS dosage from 4% to 8% increased the flexural strength at all NS and fiber levels, with improvements of approximately 2–5%, which is comparable to its effect on compressive strength (approximately 1–7%). The enhancement is attributed to a denser and more homogeneous early hydration structure resulting from controlled ettringite crystallization, which may reduce the microcracks associated with early-age shrinkage. Because flexural cracks usually originate from such pre-existing defects, reducing them increases the stress required to initiate cracking, and improved hydration around the fibers may further enhance the fiber–matrix bond. These findings suggest that AS influences flexural capacity mainly indirectly, by improving the microstructural environment in which the crack-bridging mechanism operates; direct confirmation requires shrinkage and microstructural measurements.

## RESULTS AND CONCLUSION

This study investigated the combined influence of NS, AS, and AR glass fibers on the mechanical performance of slag–cement concrete through an experimental program involving 19 mixtures. The following conclusions can be drawn:

•Partial replacement of GGBS with NS was the most influential parameter for compressive strength. Increasing the NS content from 10 to 30 kg/m³ increased the 28-day compressive strength by approximately 5.1–7.0 MPa and also increased the splitting tensile and flexural strengths, which is attributed to the filler effect, accelerated hydration, and pozzolanic formation of additional

C–S–H.

•Increasing the AS dosage from 4% to 8% increased the compressive and flexural strengths by approximately 1–7% and 2–5%, respectively, without any strength reduction, which is attributed to controlled early ettringite formation.

•AR glass fibers had a moderate effect on compressive strength but governed tensile and flexural performance: increasing the fiber content from 0.4% to 0.8% increased the splitting tensile and flexural strengths by approximately 16–21%.

•The 30NS-8AS-0.8F mixture achieved the best performance, with a 28-day compressive strength of 63.64 MPa, a splitting tensile strength of 6.6 MPa, and a flexural strength of 11.0 MPa, corresponding to increases of approximately 41%, 74%, and 77% over the control mixture.

From an engineering perspective, the investigated concrete shows potential for structural elements in urban infrastructure, such as high-rise buildings, bridge decks, and precast components, where high mechanical performance is required. Its suitability for aggressive environments should be confirmed through durability and long-term performance testing.

## REFERENCES


*Afroughsabet, V., & Teng, S. (2020). Experiments on drying shrinkage and creep of high performance hybrid-fiber-reinforced concrete. Cement and Concrete Composites, 106, 103481.*

*ASTM International. (2011). Standard specification for Portland cement (ASTM C150/C150M-11). ASTM International.*

*ASTM International. (2012). Standard practice for making and curing concrete test specimens in the laboratory (ASTM C192/C192M-12). ASTM International.*

*ASTM International. (2016). Standard test method for flexural strength of concrete (using simple beam with center-point loading) (ASTM C293/C293M-16). ASTM International.*

*ASTM International. (2017). Standard test method for splitting tensile strength of cylindrical concrete specimens (ASTM C496/C496M-17). ASTM International.*

*Bentur, A., & Mindess, S. (2007). Fibre Reinforced Cementitious Composites (2nd ed.). CRC Press.*

*British Standards Institution. (2019). Testing hardened concrete, Compressive strength of test specimens (BS EN 12390-3:2019). BSI.*

*British Standards Institution. (2021). Testing hardened concrete Shape, dimensions and other requirements for specimens and moulds (BS EN 12390-1:2021). BSI.*

*Choi, W.-C., & Yun, H.-D. (2013). Effect of expansive admixtures on the shrinkage and mechanical properties of high-performance fiber-reinforced cement composites. The Scientific World Journal, 2013, 418734. https://doi.org/10.1155/2013/418734*

*Ghafari, E., Costa, H., & Júlio, E. (2015). Critical review on eco-efficient ultra high performance concrete enhanced with nano-materials. Construction and Building Materials, 101, 201-208.*

*Hiew, S. Y., Teoh, K. B., Wong, H. S., Banthia, N., & Yoo, D. Y. (2026). Recent advances in low-carbon ultra-high-performance concrete: materials, mechanisms, and sustainability perspectives. npj Materials Sustainability, 4(1), 3.*

*Hussein, T., Kurda, R., Mosaberpanah, M., & Alyousef, R. (2022). A review of the combined effect of fibers and nano materials on the technical performance of mortar and concrete. Sustainability, 14(6), 3464.*

*Khan, K., Ahmad, W., Amin, M. N., & Nazar, S. (2022). Nano-silica-modified concrete: A bibliographic analysis and comprehensive review of material properties. Nanomaterials, 12(12), 1989. https://doi.org/10.3390/nano12121989*

*Li, J., & Yao, Y. (2001). A study on creep and drying shrinkage of high performance concrete. Cement and Concrete Research, 31(8), 1203-1206.*

*Mehdipour, I., & Khayat, K. H. (2018). Enhancing the performance of calcium sulfoaluminate blended cements with shrinkage reducing admixture or lightweight sand. Cement and Concrete Composites, 87, 29-43.*

*Nazari, A., Amirkardoust, A., & Shayegan, D. S. (2026). Experimental evaluation of strength performance of autogenous self-healing concrete under the effect of microsilica addition. Scientific Reports.*

*Piao, R., Oh, T., Kim, G. W., Choi, H. J., Banthia, N., & Yoo, D. Y. (2023). Enhanced microstructure and mechanical properties of cementless*

*ultra-high-performance fiber-reinforced alkali-activated concrete with silicon dioxide nanoparticles. Construction and Building Materials, 398, 132514.*

*Qadri, F., Nikumbh, R. K., & Jones, C. (2024). Freeze–thaw durability and shrinkage of calcium sulfoaluminate cement concrete with internal curing. Journal of Materials in Civil Engineering, 36(12), 04024422.*

*Raghav, M., Park, T., Yang, H. M., Lee, S. Y., Karthick, S., & Lee, H. S. (2021). Review of the effects of supplementary cementitious materials and chemical additives on the physical, mechanical and durability properties of hydraulic concrete. Materials, 14(23), 7270.*

*Raveendran, N., & Krishnan, V. (2025). Engineering performance and environmental assessment of sustainable concrete incorporating nano silica and metakaolin as cementitious materials. Scientific reports, 15(1), 1482.*

*Sirtoli, D., Wyrzykowski, M., Riva, P., & Lura, P. (2020). Autogenous and drying shrinkage of mortars based on Portland and calcium sulfoaluminate cements. Materials and Structures, 53(5), 126.*

*Sirtoli, D., Wyrzykowski, M., Riva, P., Tortelli, S., Marchi, M., & Lura, P. (2019). Shrinkage and creep of high-performance concrete based on calcium sulfoaluminate cement. Cement and Concrete Composites, 98, 61-73.*

*Tahwia, A. M., Elgendy, G. M., & Amin, M. (2022). Mechanical properties of affordable and sustainable ultra-high-performance concrete. Case Studies in Construction Materials, 16, e01069.*

*Vargas, J. F. T., Alvansazyazdi, M., & Castañeda, A. A. B. (2024). Study of an Environmentally Friendly High-Performance Concrete (HPC) Manufactured with the Incorporation of a Blend of Micro-Nano Silica. Eídos, 17(24), 95-110.*

*Wang, S., & Sadeghzadeh, S. M. (2025). Enhancing the Performance of Ultra-High-Performance Concrete Using Dendritic Fibrous $FeNi_3$ Nanoparticles: A Magnetically Active and Structurally Reinforcing Additive. Case Studies in Construction Materials, e05451.*

*Wang, X. Q., Chow, C. L., & Lau, D. (2024). Multiscale perspectives for advancing sustainability in fiber reinforced ultra-high performance concrete. Npj Materials Sustainability, 2(1), 13.*

*Wang, X., Wu, D., Zhang, J., Yu, R., Hou, D., & Shui, Z. (2021). Design of sustainable ultra-high-performance concrete: A review. Construction and Building Materials, 307, 124643.*

*Xuan, M. Y., & Wang, X. Y. (2022). Multi-technique investigation regarding the impact of cellulose nanofibers on ultra-high-performance concrete at the macroscopic and microscopic levels. Construction and Building Materials, 327, 126936.*

COPYRIGHTS

©2023 The author(s). This is an open access article distributed under the terms of the Creative Commons Attribution (CC BY 4.0), which permits unrestricted use, distribution, and reproduction in any medium, as long as the original authors and source are cited. No permission is required from the authors or the publishers.

HOW TO CITE THIS ARTICLE

Hojati, A., Amirkardoust, A., Sedaghat Shayegan, D. & Sistaninejad, R. (2026). Assessment of Sustainable High-performance Cementitious Concrete Incorporating Nano silica and Aluminum Sulphate for Multiscale Urban Engineering Application. (e743388). International Journal of Urban Management and Energy Sustainability, 7(3), e743388

DOI:10.22034/ijumes.2026.743388